Journal of Biomechanics 169 (2024) 112156

Contents lists available at ScienceDirect

Journal of Biomechanics

journal homepage: www.elsevier.com/locate/jbiomech

Disturbed fluid flow reinforces endothelial tractions and intercellular stresses

Jingwen Wu, R.L. Steward Jr *

Department of Mechanical and Aerospace Engineering, University of Central Florida, Orlando, FL, United States

ARTICLE INFO

Keywords:
Endothelial cells
Disturbed flow
Tractions
Intercellular stresses

ABSTRACT

Disturbed fluid flow is well understood to have significant ramifications on endothelial function, but the impact disturbed flow has on endothelial biomechanics is not well understood. In this study, we measured tractions, intercellular stresses, and cell velocity of endothelial cells exposed to disturbed flow using a custom-fabricated flow chamber. Our flow chamber exposed cells to disturbed fluid flow within the following spatial zones: zone 1 (inlet; length 0.676–2.027 cm): 0.0037 ± 0.0001 Pa; zone 2 (middle; length 2.027–3.716 cm): 0.0059 ± 0.0005 Pa; and zone 3 (outlet; length 3.716–5.405 cm): 0.0051 ± 0.0025 Pa. Tractions and intercellular stresses were observed to be highest in the middle of the chamber (zone 2) and lowest at the chamber outlet (zone 3), while cell velocity was highest near the chamber inlet (zone 1), and lowest near the middle of the chamber (zone 2). Our findings suggest endothelial biomechanical response to disturbed fluid flow to be dependent on not only shear stress magnitude, but the spatial shear stress gradient as well. We believe our results will be useful to a host of fields including endothelial cell biology, the cardiovascular field, and cellular biomechanics in general.

1. Introduction

Within the blood vessel, endothelial cells (ECs) may be exposed to disturbed flow or undisturbed flow. On the one hand, undisturbed flow occurs in the straight part of the blood vessel, has uniform flow direction, is frequently associated with high wall shear stress, and is barrier protective. On the other hand, disturbed flow occurs primarily in the bifurcated regions of the blood vessel, separates from the wall, becomes multidirectional, and generally consists of spatially irregular flow profiles with low wall shear stress (Malek et al., 1999). In general, disturbed fluid flow has been reported to consist of low fluid shear stress much less than 4 dyn/cm^2 (0.4 Pa) (Malek et al., 1999) and is known to be barrier disruptive as it induces upregulation of pro-inflammatory genes and proteins that promote endothelial dysfunction (Davignon & Ganz, 2004; Endemann & Schiffrin, 2004; M. A. Gimbrone et al., 2000; Nam et al., 2009; Souilhol et al., 2018). Endothelial dysfunction is defined as the endothelium's diminished capacity to perform routine vascular function, such as nitric oxide production, vasoconstriction, vasodilation, and barrier function (Moncada & Higgs, 2006; Ongini et al., 2004; Pacher et al., 2007; Widlansky et al., 2003). In addition, endothelial dysfunction has important implications in hemostasis and thrombosis regulation as well as acute chronic inflammation within the blood vessel (M. A. Gimbrone & García-Cardeña, 2016). Numerous studies have demonstrated endothelial dysfunction to have a profound impact on numerous cardiovascular diseases including hypertension, and atherosclerosis, for example (Widlansky et al., 2003).

In addition to the cardiovascular pathological ramifications of disturbed flow mentioned above, disturbed flow also impacts physiological endothelial processes such as proliferation and angiogenesis. For example, Chiu et al. (Chiu & Chien, 2011) demonstrated disturbed flow to cause activation of the extracellular signal-regulated kinases (ERK), which is suggested to be regulated by inhibiting the p21^{CIP1}-suppression of cyclin-dependent kinase activity for $G_0/G_{1\text{-}S}$ transition. This allowed more cells to enter the cell cycle and arrest most cells in the $G_0/G_{1\text{-}S}$ phase, resulting in high proliferation and angiogenesis (Akimoto et al., 2000; Davies, 2000; Lin et al., 2000; Zeng et al., 2003). In addition, Chien et al. (Chien, 2008) demonstrated endothelial cells exposed to disturbed flow to activate proinflammatory and proliferative pathways, subsequently resulting in altered vascular permeability to lipoproteins, enhanced mononuclear leukocyte recruitment and increased smooth muscle cell proliferation, thus promoting atherogenesis (J. Gimbrone, 1999; M. A. Gimbrone et al., 1997; M. A. Gimbrone & García-Cardeña, 2016; Kumar et al., 2014; Nigro et al., 2011; Resnick & Cimbrone, 1995). In general, abnormal EC behavior arising from the disturbed flow

* Corresponding author.
E-mail address: rstewardjr@ucf.edu (R.L. Steward).

https://doi.org/10.1016/j.jbiomech.2024.112156
Accepted 14 May 2024
Available online 15 May 2024

studies previously mentioned demonstrate disturbed flow's impact on cardiovascular disease observed from a biological perspective.

Disturbed flow has also been suggested to have biomechanical impacts on the endothelium, specifically cell-generated mechanical stresses such at the cell-matrix and cell–cell level. One mechanism by which ECs and all anchorage-dependent cells to respond biomechanically to their microenvironment requires them to generate actomyosin contractile forces on their underlying extracellular matrix (ECM)(Patel et al., 2019; Tang et al., 2014; Wang & Lin, 2007). These cell-matrix forces, which we call tractions, are important in cell migration and proliferation. Furthermore, tractions have been suggested to be important in a host of mechanics-related pathologies such as angiogenesis, cancer metastasis, and leucocyte extravasation, for example (Han et al., 2012; Oakes et al., 2018; Soon et al., 2015; Trepat et al., 2009; Wagenseil & Mecham, 2012). In addition to the tractions exerted on the underlying matrix, there also exist mechanical stresses exerted at the cell–cell level through cell junctions, which we known as intercellular stresses (Patel et al., 2019; Tang et al., 2014; Wang & Lin, 2007). Intercellular stresses, have been suggested to also be important in collective cell migration and endothelial mechanical barrier function.

To measure tractions and intercellular stresses, we used traction force microscopy (TFM) (Butler et al., 2002; Franck et al., 2011) and monolayer stress microscopy (MSM), respectively (Tambe et al., 2013). Previous studies investigating disturbed flow on the endothelium and the biomechanical forces mentioned above have yielded diverse results. Perrault et al. (Perrault et al., 2015) found that human umbilical vein endothelial cells (HUVECs) exposed to a low, unidirectional, undisturbed flow resulted in increased in tractions and intercellular stresses, while Ting et al. (Ting et al., 2012) reported human pulmonary artery endothelial cells (HPAECs) exposed to a multidirectional, disturbed flow to yield lower tractions when compared to static conditions along with decreased size in adherens junctions and tight junctions. The link between disturbed flow, tractions, and intercellular stresses needs to be clearly understood. Therefore, to shed light on this obscure phenomenon between disturbed flow and endothelial cell mechanics, we examined tractions and intercellular stresses of endothelial cells exposed to the disturbed flow of variable spatial regimes.

2. Materials and methods

2.1. Flow chamber

A disturbed flow chamber was fabricated in-house for our disturbed flow experiments. The device consisted of a top and bottom cover of plexiglass, one main chamber made with Delrin$^{(R)}$, and two pieces of gaskets on the top and bottom (Fig. 1). The flow chamber has a height of 1.50 cm, a width of 5.00 cm, and a length of 8.99 cm. To create a disturbed flow condition, our chamber has an inlet height of 1.22 cm and an outlet height of 0.38 cm (Fig. 1).

2.2. Computational fluid dynamics modeling

A three-dimensional (3D) flow chamber model was designed using SolidWorks CAD software. This 3D model was imported into the Star-CCM + software for Computational Fluid Dynamic (CFD) simulations. Fluid properties of water at 37 °C were used. Furthermore, the experimental flow rate of 10 mL/min was used for the inlet velocity and outlet pressure of 0 Pa under non-slip boundary conditions. A mesh size is 0.1 cm using volumetric trimmer elements with selected prism layer and thickness (Fig. 2). Guided by results from our CFD model, we analyzed cells within three flow zones which we defined spatially as follows: zone 1 (inlet; length 0.68–2.02 cm and width 5 cm), zone 2 (middle; length 2.023–3.72 cm and width 5 cm), and zone 3 (outlet; length 3.72–5.41 cm and width 5 cm) (Fig. 3).

2.3. Cell culture

Human Umbilical Vein Endothelial Cells (HUVECs) were purchased from ThermoFisher and cultured in medium 200 (Fisher Scientific) supplemented with large vessel endothelial supplement (LVES) (Fisher

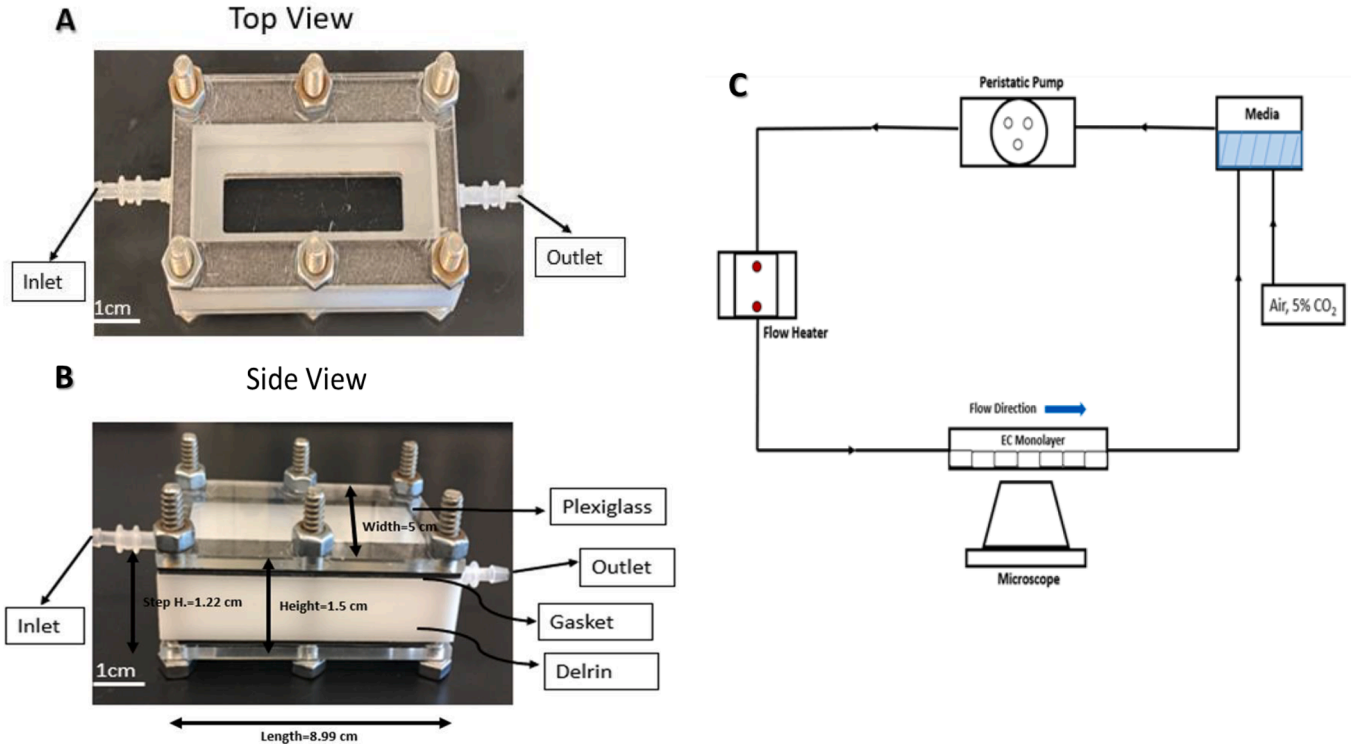

Fig. 1. A) Top view and B) Side view of the 3D flow chamber. C) Schematic drawing of the fluid shear experiment.

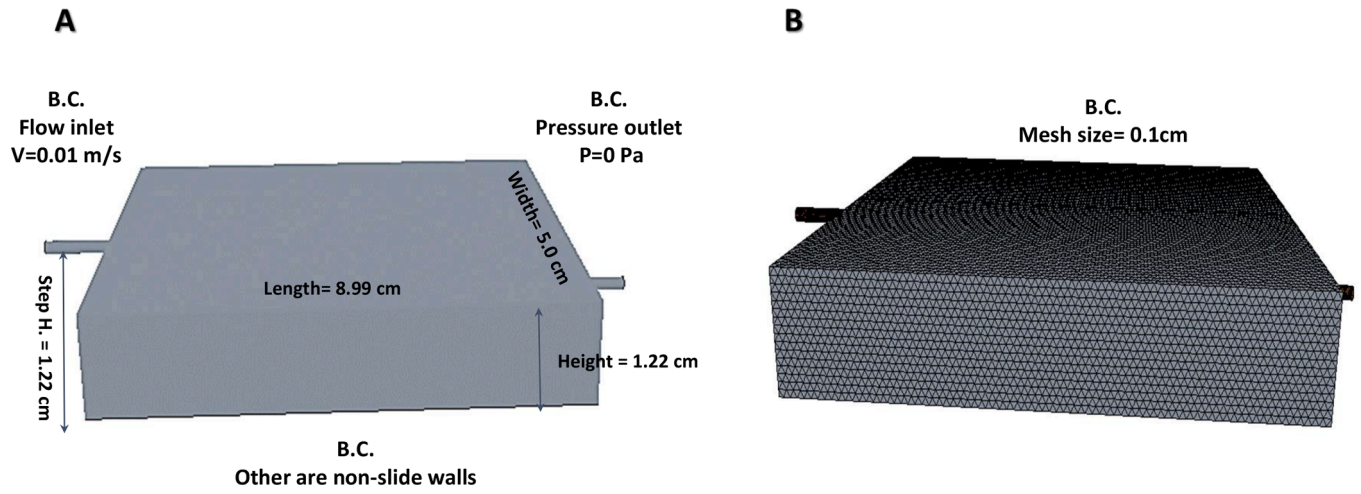

Fig. 2. A) Boundary and B) mesh condition of the 3D flow chamber.

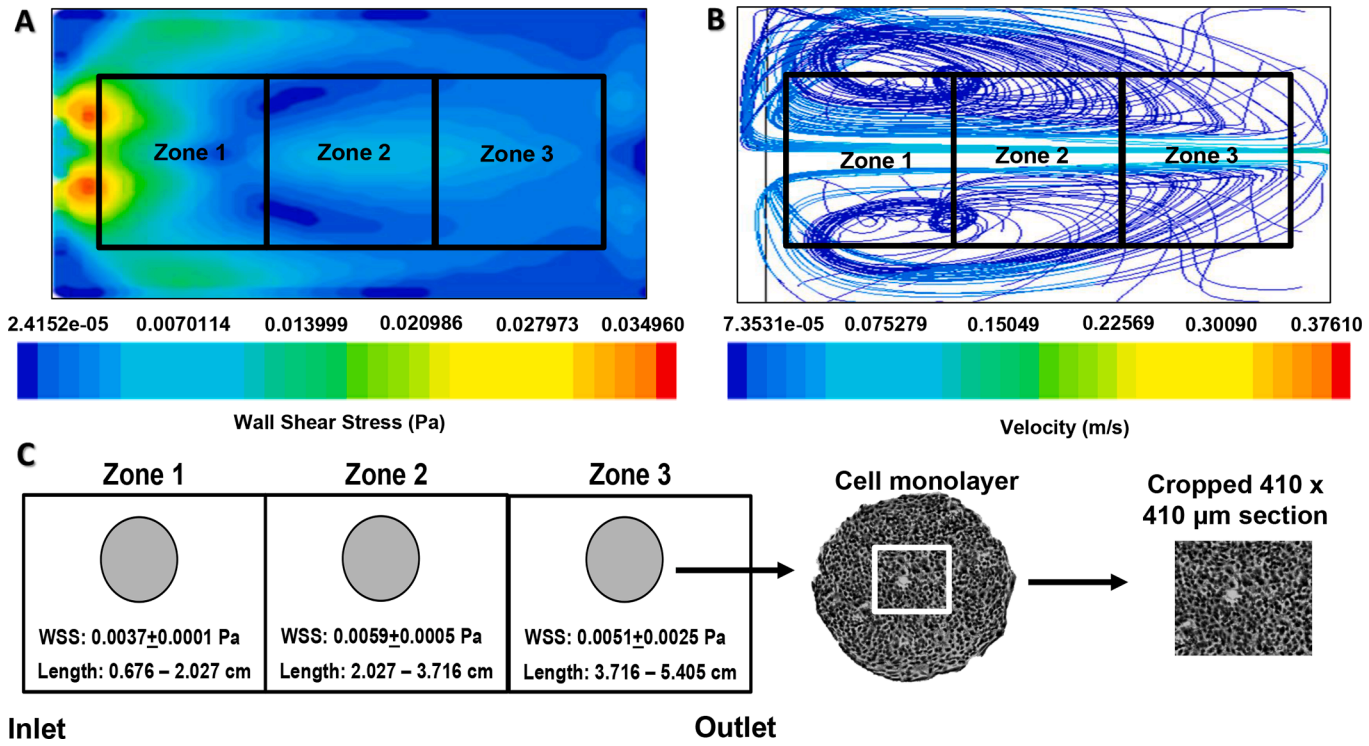

Fig. 3. CFD simulations of the 3D flow chamber A) wall shear stress (WWS) (Pa). B) flow streamline (m/s) magnitude distribution with zone 1, 2, and 3. C) Cell zone 1, 2 and, 3 with WWS and phase contrast image of micropatterned monolayer at the bottom of the 3D flow chamber.

Scientific) and 1 % penicillin–streptomycin (Corning) on 0.1 % gelatin (Sigma-Aldrich) coated flasks. Cells were cultured at 37 °C and 5 % CO_2.

2.4. Polyacrylamide (PA) gel preparation

PA gels were fabricated as previously described by us (R. Steward et al., 2015). In brief, a microscope glass slide (ThemoFisher) was treated with NaOH (for 1 h), 97 % Aminopropytrimethoxisilane (ALDRICH Chemistry, for 6 min), and 0.25 % Glutaraldehyde (ThermoFisher), for 30 min) before gel polymerization. The PA gel solution (E = 1.2Kpa)(M. A. Gimbrone & García-Cardeña, 2016) was prepared by mixing Ultra-pure Water, 40 % Acrylamide (Bio-Rad), 2 % Bis-Acrylamide (Bio-Rad), and 0.5 µm diameter red fluorescent beads (Invitrogen). In addition, Ammonium Persulfate and TEMED (N, N, N', N'-tetramethylethane-1,2-diamine) were added to polymerize the PA gel on the treated glass slides to yield a soft, elastomeric substrate.

2.5. SANPAH burning and collagen coating of PA hydrogels

Additional treatments of PA hydrogel with a bifunctional reagent N-succinimidyl 6-(4′-azido-2′-nitrophenylamino) hexanoate (SANPAH) burning and Collagen I coating were required before seeding the cells on the PA gel. These two additional treatments primarily aimed to functionalize the PA gels for collagen coating and subsequent cell seeding on the gel surface. SANPAH was dissolved in 0.1 M HEPES buffer solution (Fisher Scientific) to a final concentration of 10 mM, placed on the surface of the gel, and subsequently exposed to UV light for 8–10 min. Afterward, gels were coated with 0.1 mg/ml of collagen I (Advanced

Biomatrix) and incubated overnight at 4 °C. The following day, excess collagen was aspirated. The gel was rinsed with phosphate-buffered saline (PBS) at least two times, and HUVECs were seeded as a 2 mm circular micropatterns on the hydrogel. HUVEC monolayers were incubated at 37 °C and 5 % CO_2 for at least 48 h before experimentation.

2.6. Disturbed flow experiment

A schematic of the experimental setup is shown in Fig. 1C. In brief, our experimental design consisted of a programmable peristaltic flow pump, an in-line solution flow heater, and a cell culture media reservoir bubbled with 5 % CO_2. Cells were exposed to a 10 mL/min flow rate for 6 h. We choose this time point as the results we report here were all reported to be statistically significant by this time point. During this time, cells were exposed to a spatially heterogeneous, fluid shear stress gradient that was as follows; 0.0037 ± 0.0001 Pa (zone 1), 0.0059 ± 0.0005 Pa (zone 2), and 0.0051 ± 0.0025 Pa (zone 3) (Fig. 3).

2.7. Time lapse microscopy experiments

Phase contrast and fluorescent images were acquired every 10 min for 6 h with a Zeiss axiovert inverted microscope and 5X objective. After 6 h, HUVEC monolayers were treated with 10 % Triton-X 100 (Thermo-Fisher) to detach cells from the gel surface to acquire stress-free images of the gel surface, which is essential for traction measurements.

2.8. Traction force microscopy (TFM) and monolayer stress microscopy (MSM)

As mentioned above, all HUVEC monolayers were seeded as 2 mm diameter, circular micropatterns. However, micropatterns have been well established to induce boundary affects. To remove any potential contribution of boundary effects to our data we analyzed traction and intercellular stress data solely within a cropped 410 × 410 μm square section within the center of the 2 mm micropattern monolayer (Fig. 3 C). TFM and MSM were used to calculate the traction and intercellular stresses exerted by endothelial cells on their substrate and between each other, respectively (Butler et al., 2002; Franck et al., 2011; R. Steward et al., 2015; R. L. Steward et al., 2010; Tambe et al., 2013). To calculate the tractions, the in-plane displacement field on the top surface of the gel was measured using a particle image velocimetry routine written in MATLAB using the following parameters: a 32 x 32 window size and 0.75 overlap. Image cross-correlation algorithm was used to calculate the associated displacements (in pixels) between a stress-free image (image taken after cell trypsinization) and a stressed image (with cells attached) (Butler et al., 2002; Franck et al., 2011; Tambe et al., 2013). Building upon traction force microscopy, monolayer stress microscopy (MSM) was used to calculate the in-plane intercellular stresses balanced by cell-substrate tractions as implied by Newton's laws (R. Steward et al., 2015; R. L. Steward et al., 2010). MSM allows us to compute the local stress tensor within the 2D monolayer, which is converted into the maximum principal stress (σ_{max}) and minimum principal stress (σ_{min}) along with the corresponding principal planes of orientation. Using the maximum and minimum principal stress we calculate the average normal intercellular stress ($\frac{\sigma_{max}+\sigma_{min}}{2}$) and maximum shear intercellular stress ($\frac{\sigma_{max}-\sigma_{min}}{2}$) at each point within the monolayer.

2.9. Cell velocity calculation

All results were analyzed over a cropped 410 × 410 μm section within the middle of the 2 mm micropattern monolayer. Cell velocity was measured using a custom-written particle image velocimetry (PIV) routine (with parameters of 32 x 32 window size and 0.75 overlap) in MATLAB to track cellular displacements from phase contrast images at two consecutive time points. The velocity map of the cells in the monolayer was calculated by averaging the change in displacements over the time interval. Cell velocity was calculated at every 10 min interval for the entire sequences of images acquired over 6 h.

2.10. Statistical significance

Each fluid shear stress zone (zone 1, zone 2, and zone 3) was tested for statistical significance by comparing measured values for tractions, intercellular stress, and cell velocity to the static condition (no fluid shear) using ANOVA. The p-values for significance were calculated with an alpha level of 0.05 (Null hypothesis rejected for $p < 0.05$).

3. Results

3.1. Tractions are highest in zone 2 and lowest in zone 3

Phase contrast images of endothelial cells after exposure to 100 min, 200 min, and 300 min are shown in Fig. 4. The spatial distributions of the tractions after six hours for zones 1–3 as well as static experiments are shown illustrated in Fig. 5. Tractions from the static experiment fluctuated around 17.96 ± 0.74 Pa. After 6 h of disturbed flow, zone 2 (middle) was observed to have the highest tractions (37.08 ± 8.67 Pa) followed by zone 1 (31.91 ± 2.43P, and zone 3, which had the lowest tractions (28.34 ± 3.05 Pa).

3.2. Intercellular stresses are highest in zone 2 and lowest in zones 3

The spatial distributions of the average normal intercellular stresses and maximum shear intercellular stress after six hours of disturbed flow are shown for zones 1–3 and static experiments in Fig. 6 and Fig. 7. The average normal stress from the static control experiment was 218.48 ± 12.40 Pa and maximum shear stress was 177.80 ± 6.50 Pa. Among the endothelial cells exposed to disturbed flow, monolayer in zone 2 (middle of chamber) were observed to have the highest average normal stresses (195.29 ± 12.70 Pa) followed by zone 1 (189.29 ± 10.59 Pa), and zone 3, which had the lowest average normal stresses (124.60 ± 8.73 Pa). The maximum shear stress was observed to be the highest in monolayers of zone 2 (108.06 ± 14.52 Pa) followed by zone 1 (95.61 ± 11.18 Pa), and zone 3, which had the lowest maximum shear stress (87.89 ± 5.87 Pa;).

3.3. Endothelial cell velocity is highest in zone 1 and lowest in zone 2

The spatial distributions of the cell velocity after six hours for chamber zone 1–3 are shown in Fig. 8A-D. The cell velocity from the static control experiment was 0.14 ± 0.01 μm/min. After 6 h of disturbed flow experiment, zone 1 was observed to have the highest cell velocity (0.79 ± 0.13 μm/min) followed by zone 3 (0.74 ± 0.14 μm/min), and zone 2, which had the lowest cell velocity (0.73 ± 0.14 μm/min). The bar plots displaying the average cell velocity with statistical significance for zone 1, 2, 3 and static are shown in Fig. 8F.

4. Discussion

The tractions, average normal stresses, and maximum shear stress were observed to be the highest in zone 2, which was in the middle of the flow chamber. We suggest this to be due to the fact that our CFD simulations indicated zone 2 to qualitatively have the most non-uniform flow streamlines patterns and overall higher wall shear stress. The cell velocity did not follow the same trend as tractions and intercellular stresses, as zone 1 was instead observed to have the highest value. Previous studies have demonstrated cell proliferation and endothelial permeability to increase when subjected to disturbed flow due to the increase of more cells entering the cell cycle from the inhibition of the $p21^{CIP1}$-suppression of cyclin-dependent kinase activity in $G_0/G_{1\text{-}S}$ transition (Akimoto et al., 2000; Davies, 2000; Lin et al., 2000; Zeng et al., 2003), also the disruption of macromolecules (e.g., I-albumin, and

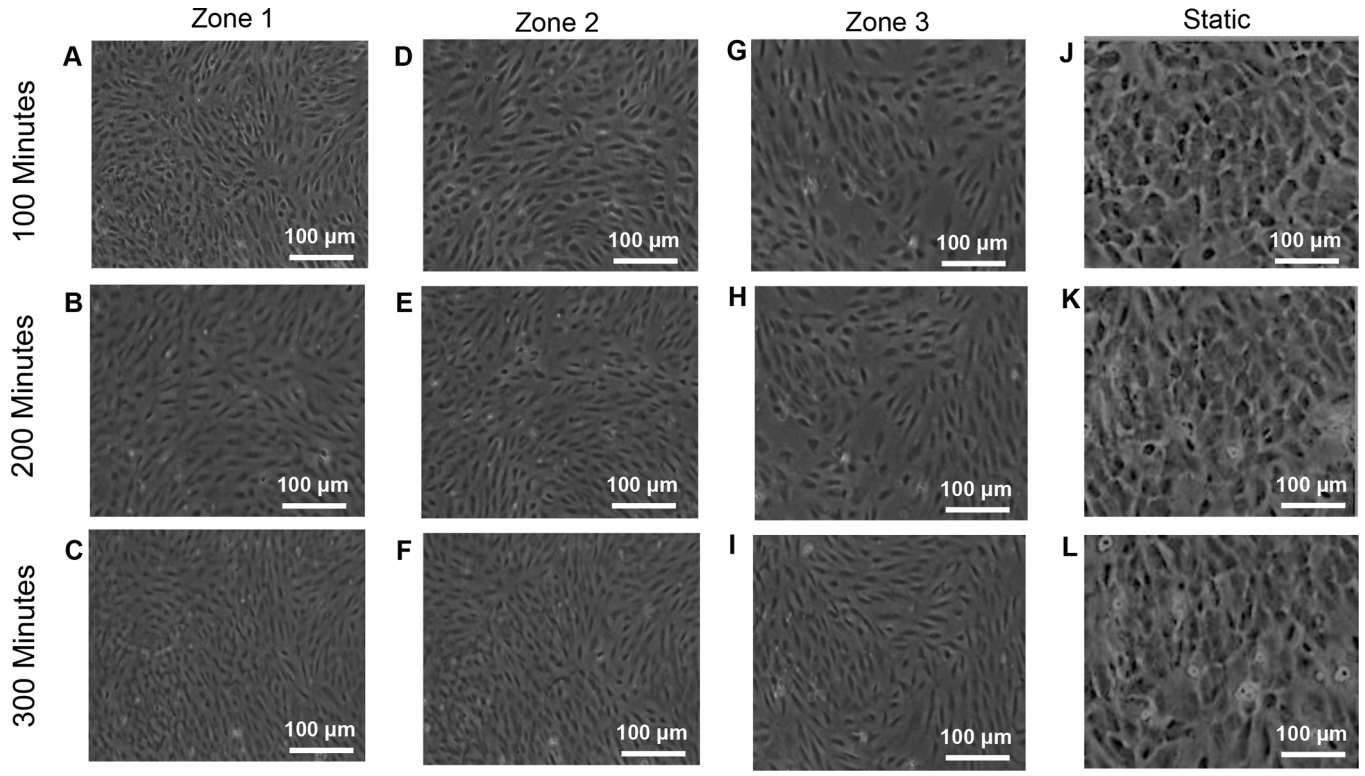

Fig. 4. A-I) Phase contrast images of endothelial cell morphology at three different time points: 100, 200, and 300 min during the fluid shear experiment. *A-C: zone 1; D-F: zone 2; G-I: zone 3; and J-L: static (no flow) condition.

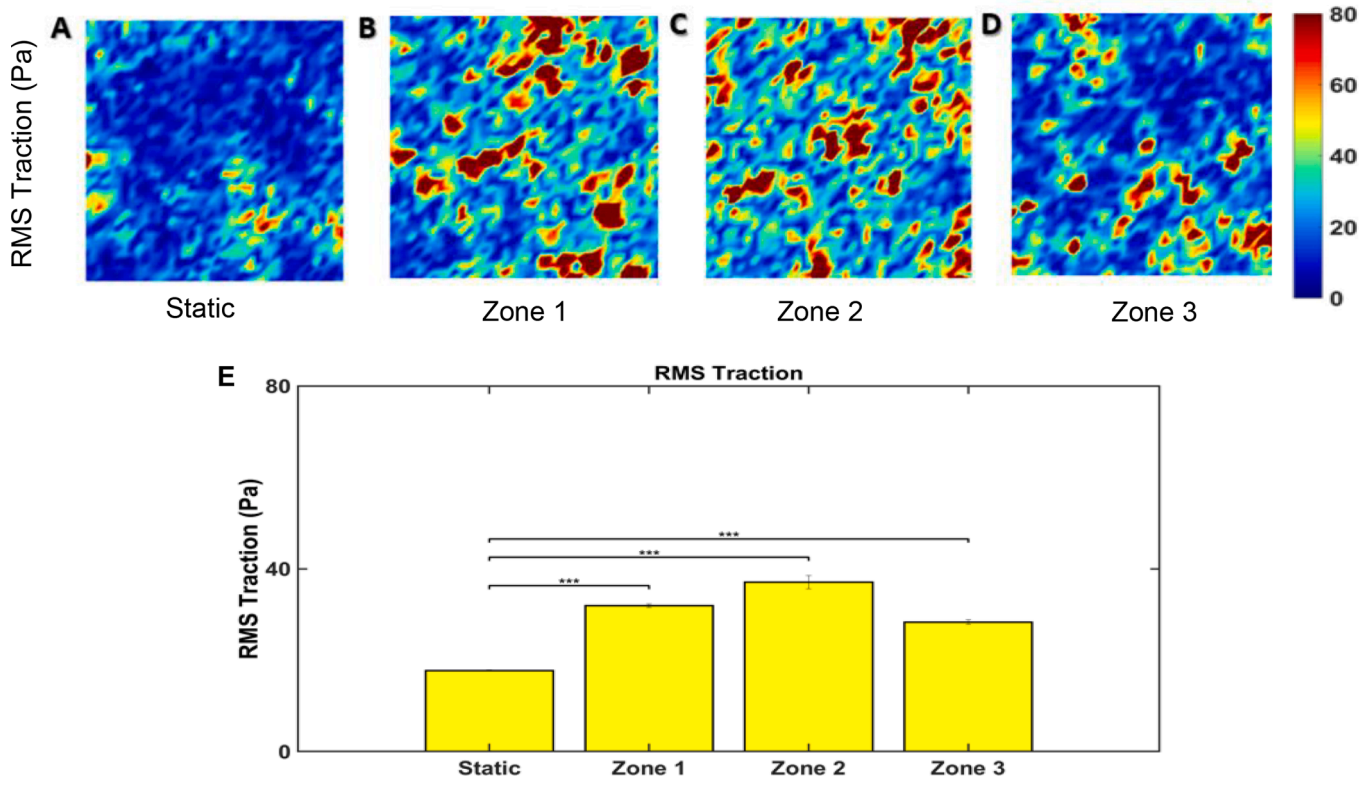

Fig. 5. RMS tractions (Pa) under (A) static conditions, (B) zone 1, (C) zone 2, and (D) zone 3 at six hours. (E) Bar plot of rms tractions (Pa) for zones 1–3 and static conditions.* Represents statistical significance (* p <= 0.05; ** p <= 1E-2; *** p<= 1E-3, no star p > 0.05).

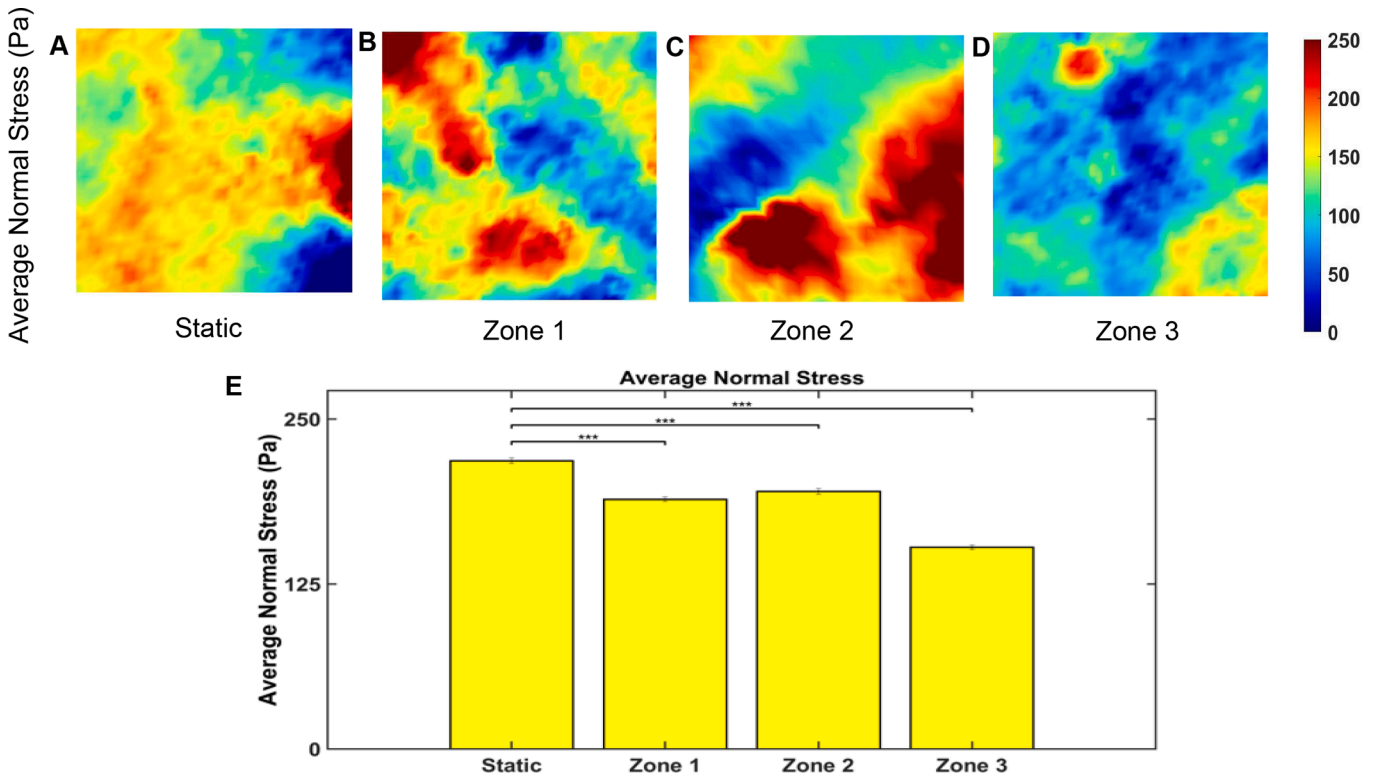

Fig. 6. Average normal stress (Pa) under (A) static conditions, (B) zone 1, (C) zone 2, and (D) zone 3 at six hours. (E) Bar plot of average normal stress (Pa) for zones 1–3 and static conditions. * Represents statistical significance (* p <= 0.05; ** p <= 1E-2; *** p<= 1E-3, no star p > 0.05).

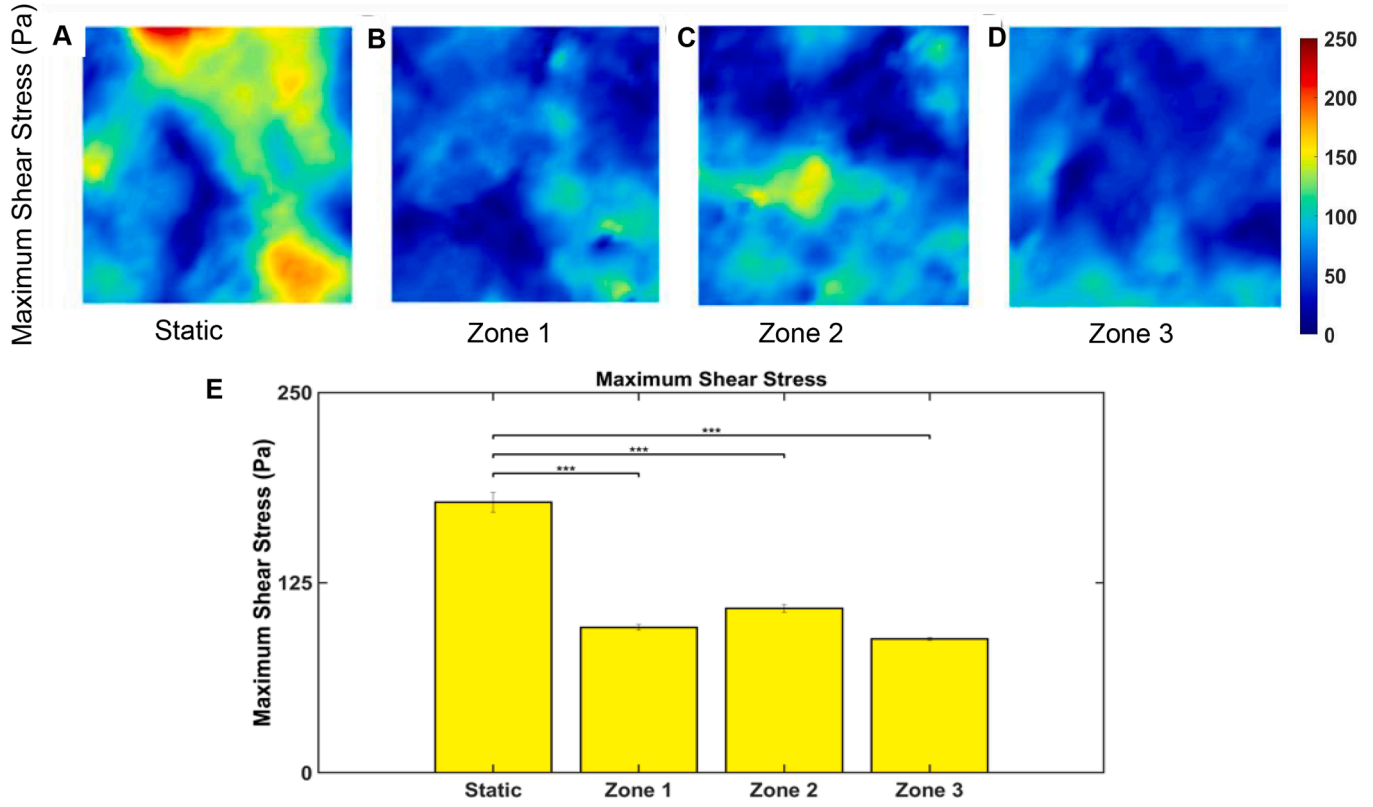

Fig. 7. Maximum shear stress under (A) static conditions, (B) zone 1, (C) zone 2, and (D) zone 3 at six hours. (E) Bar plot of maximum shear stress (Pa) for zones 1–3 and static conditions.* Represents statistical significance (* p <= 0.05; ** p <= 1E-2; *** p<= 1E-3, no star p > 0.05).

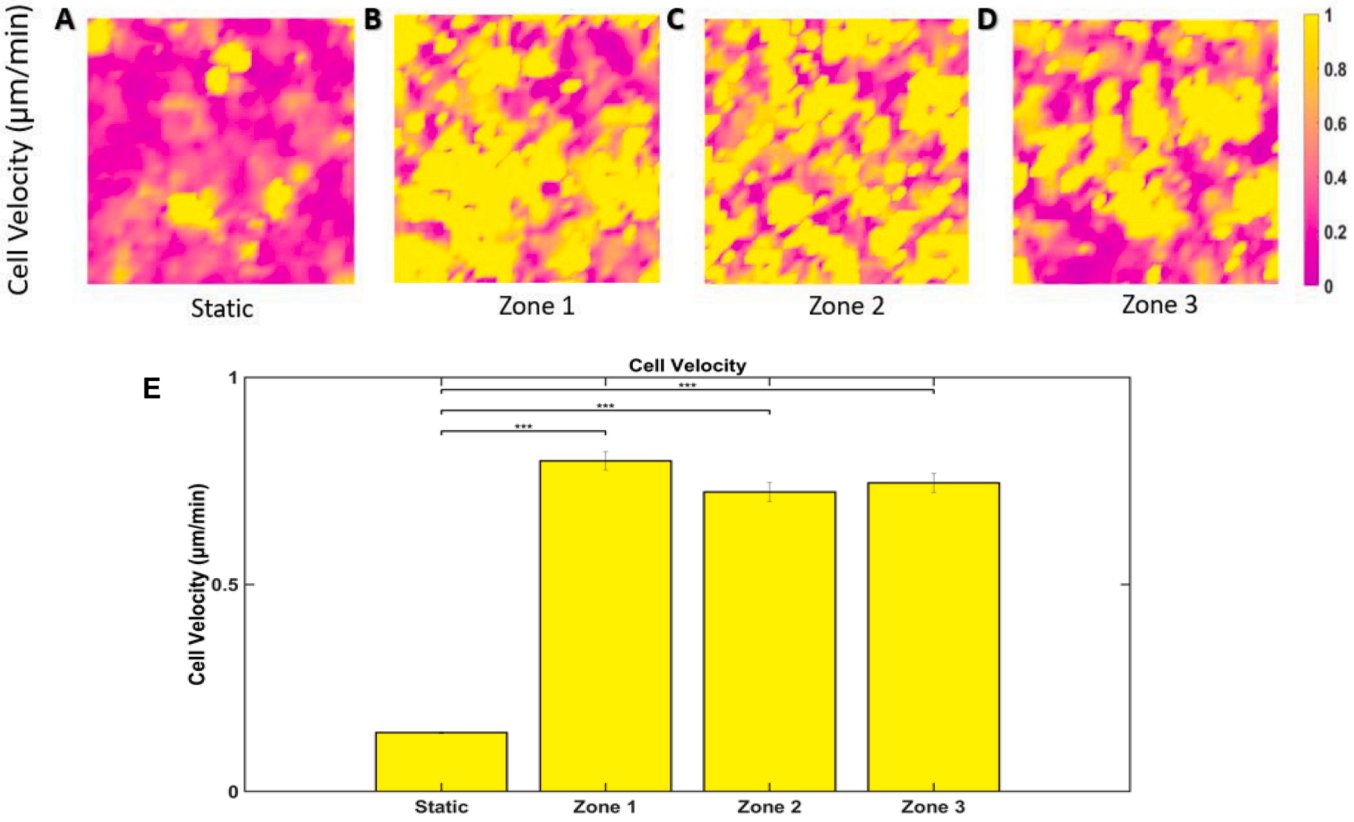

Fig. 8. Cell velocity under (A) static conditions, (B) zone 1, (C) zone 2, and (D) zone 3 at six hours. (E) Bar plot of cell velocity (Pa) for zones 1–3 and static conditions.* Represents statistical significance (* p <= 0.05; ** p <= 1E-2; *** p<= 1E-3, no star p > 0.05).

low-density lipoprotein (LDL)) and intercellular junctional proteins (e.g., connexins (Cx) and vascular endothelial (VE)-cadherin) (Brooks et al., 2002; Chiu & Chien, 2011). We propose that zone 2 has the highest tractions, and intercellular stresses due to the increased endothelial cell turnover and higher proliferation rate that other groups have reported under disturbed flow (Akimoto et al., 2000; Brooks et al., 2002; Chiu & Chien, 2011; Davies, 2000; Lin et al., 2000; Zeng et al., 2003). (Zhang et al., 1999).

Ting et. al. reported cells under undisturbed flow to exert higher tractions and intercellular forces and cells exposed to disturbed flow to exert lower tractions and intercellular forces when compared to static conditions. While we do not investigate undisturbed flow in this study, we do report cells exposed to disturbed flow to exert higher tractions, but lower intercellular stresses when compared to static conditions. We believe these somewhat divergent results to be attributed to the following key differences 1) Ting et. al. exposed cells to a wall shear stress between −2.4 – 1.9 Pa, while we exposed cells to a much lower 0.004–0.005 Pa and 2) Ting et. al. cultured cells on a 160 x 160 μm square, while we cultured cells on a 2 mm circular pattern, each reflecting key experimental parameters that influenced our results. Taken into account or study as well as Ting et. al. we believe together these studies can be used to better understand the impact disturbed flow has on endothelial mechanics. Furthermore, the statistical single ANOVA tests have shown that the traction, intercellular stresses, and cell velocity obtained from the fluid shear experiment are statistically significant. Our results demonstrated that wall shear stress magnitude and flow direction has a significant influence on tractions and intercellular stresses. Both tractions and intercellular stresses have been suggested to be critical to normal vascular function therefore, the results we present here have implications into numerous vascular pathologies such as stroke and hypertension, for example.

5. Conclusion

In this paper, we investigated endothelial mechanics, such as traction and intercellular stresses, with the application of disturbed flow conditions. In general, cells have been found to be sensitive to flow direction and we believe this may explain the results we report here. In addition to flow magnitude and direction, (Gabriel et al., 2017) and (He and Ku) have also reported additional disturbed flow properties including Oscillatory Shear Index and Oscillatory Kinetic Energy Index to also influence vascular response as well. While beyond the scope of this paper we believe this should be investigated for future works. In addition, we have published previous works (Ranadewa et al., 2021) demonstrating the effects of fluid flow on endothelial cell–cell junction and cytoskeletal structure. Our results revealed endothelial cells exposed to oscillatory flow (a form of disturbed flow) to exhibit unique structural changes in in ZO-1, Claudin-5, JAM-A, VE-Cadherin, and F-actin. The results previously mentioned suggested endothelial cell–cell junction and cytoskeletal structural reorganization to potentially in part explain the results we report here. We believe these findings will have significant implications in studying biomechanical processes involved in cardiovascular diseases such as atherosclerosis, which have higher risks associated with the experiences of disturbed blood flow of human blood vessels. For example, numerous studies have shown that atherosclerosis lesions most likely occur at the curvature or branches of the blood vessel (M. A. Gimbrone & García-Cardeña, 2016; Moncada & Higgs, 2006; Ongini et al., 2004; Pacher et al., 2007; Widlansky et al., 2003). The regions that experienced disturbed flow generally experienced low wall shear stress and high endothelial permeability (Brooks et al., 2002; Chiu & Chien, 2011). Therefore, we believe our results will yield opportunities to better understand the endothelium's pathology and physiology from a biomechanical perspective.

CRediT authorship contribution statement

Wu. Jingwen: Writing – original draft, Methodology, Data curation. **R.L. Steward:** Writing – review & editing, Supervision, Methodology.

Declaration of competing interest

The authors declare that they have no known competing financial interests or personal relationships that could have appeared to influence the work reported in this paper.

Acknowledgments

This material is based on work supported by the National Science Foundation CAREER Award under Grant No. 2045750. A special thanks to Sean Beverung for the help with static control data organizing.

Appendix A. Supplementary data

Supplementary data to this article can be found online at https://doi.org/10.1016/j.jbiomech.2024.112156.

References

Akimoto, S., Mitsumata, M., Sasaguri, T., Yoshida, Y., 2000. Laminar shear stress inhibits vascular endothelial cell proliferation by inducing cyclin-dependent kinase inhibitor p21(Sdi1/Cip/Waf1). Circ. Res. 86 (2).
Brooks, A.R., Lelkes, P.I., Rubanyi, G.M., 2002. Gene expression profiling of human aortic endothelial cells exposed to disturbed flow and steady laminar flow. Physiol. Genomics 2002 (9).
Butler, J.P., Toli-Nørrelykke, I.M., Fabry, B., Fredberg, J.J., 2002. Traction fields, moments, and strain energy that cells exert on their surroundings. Am. J. Physiol. Cell Physiol. 282 (3), 51–53.
Chien, S., 2008. Effects of disturbed flow on endothelial cells. Ann. Biomed. Eng. 36 (4).
Chiu, J.J., Chien, S., 2011. Effects of disturbed flow on vascular endothelium: pathophysiological basis and clinical perspectives. In Physiological Reviews 91 (1).
Davies, P.F., 2000. Spatial hemodynamics, the endothelium, and focal atherogenesis: a cell cycle link? In Circulation Research 86 (2).
Davignon, J., Ganz, P., 2004. Role of endothelial dysfunction in atherosclerosis. In Circulation 109 (23). https://doi.org/10.1161/01.cir.0000131515.03336.f8.
Endemann, D.H., Schiffrin, E.L., 2004. Endothelial dysfunction. J. Am. Soc. Nephrol. 15 (8).
Franck, C., Maskarinec, S.A., Tirrell, D.A., Ravichandran, G., 2011. Three-dimensional traction force microscopy: a new tool for quantifying cell-matrix interactions. PLoS One 6 (3).
Gabriel, S.A., Ding, Y., Feng, Y., 2017. Quantifying the influence of oscillatory flow disturbances on blood flow. J Theor Biol 430, 195–206.
Gimbrone, J., 1999. Vascular endothelium, hemodynamic forces, and atherogenesis. In. Am. J. Pathol. 155 (1).
Gimbrone, M.A., García-Cardeña, G., 2016. Endothelial cell dysfunction and the pathobiology of atherosclerosis. Circ. Res. 118 (4).
Gimbrone, M.A., Nagel, T., Topper, J.N., 1997. Biomechanical activation: an emerging paradigm in endothelial adhesion biology. J. Clin. Investig. 99 (8).
Gimbrone, M.A., Topper, J.N., Nagel, T., Anderson, K.R., Garcia-Cardeña, G., 2000. Endothelial dysfunction, hemodynamic forces, and atherogenesis. Ann. N. Y. Acad. Sci. 902.
Han, S.J., Bielawski, K.S., Ting, L.H., Rodriguez, M.L., Sniadecki, N.J., 2012. Decoupling substrate stiffness, spread area, and micropost density: a close spatial relationship between traction forces and focal adhesions. Biophys. J . 103 (4).
Kumar, S., Kim, C.W., Simmons, R.D., Jo, H., 2014. Role of flow-sensitive microRNAs in endothelial dysfunction and atherosclerosis mechanosensitive athero-miRs. Arterioscler. Thromb. Vasc. Biol. 34 (10).
Lin, K., Hsu, P.P., Chen, B.P., Yuan, S., Usami, S., Shyy, J.Y.J., Li, Y.S., Chien, S., 2000. Molecular mechanism of endothelial growth arrest by laminar shear stress. PNAS 97 (17).
Malek, A.M., Alper, S.L., Izumo, S., 1999. Hemodynamic shear stress and its role in atherosclerosis. J. Am. Med. Assoc. 282 (21).
Moncada, S., Higgs, E.A., 2006. Nitric oxide and the vascular endothelium. Handb. Exp. Pharmacol. 176 (PART1).
Nam, D., Ni, C.W., Rezvan, A., Suo, J., Budzyn, K., Llanos, A., Harrison, D., Giddens, D., Jo, H., 2009. Partial carotid ligation is a model of acutely induced disturbed flow, leading to rapid endothelial dysfunction and atherosclerosis. Am. J. Physiol. Heart Circ. Physiol. 297 (4).
Nigro, P., Abe, J.I., Berk, B.C., 2011. Flow shear stress and atherosclerosis: a matter of site specificity. In Antioxidants and Redox Signaling 15 (5).
Oakes, P.W., Bidone, T.C., Beckham, Y., Skeeters, A.V., Ramirez-San Juan, G.R., Winter, S.P., Voth, G.A., Gardel, M.L., 2018. Lamellipodium is a myosin-independent mechanosensor. PNAS 115 (11).
Ongini, E., Impagnatiello, F., Bonazzi, A., Guzzetta, M., Govoni, M., Monopoli, A., Del Soldato, P., Ignarro, L.J., 2004. Nitric oxide (NO)-releasing statin derivatives, a class of drugs showing enhanced antiproliferative and antiinflammatory properties. PNAS 101 (22).
Pacher, P., Beckman, J.S., Liaudet, L., 2007. Nitric oxide and peroxynitrite in health and disease. In Physiological Reviews 87 (1).
Patel, G., Xu, N., Nguyen, A., Alvarez, D.F., Fredberg, J.J., Stevens, T., Tambe, D.T., 2019. Mechanical signaling in a pulmonary microvascular endothelial cell monolayer. Biochem. Biophys. Res. Commun. 519 (2).
Perrault, C.M., Brugues, A., Bazellieres, E., Ricco, P., Lacroix, D., Trepat, X., 2015. Traction forces of endothelial cells under slow shear flow. Biophys. J . 109 (8).
Ranadewa, D., Wu, J., Subramanianbalachandar, V.A., Steward Jr., R.L., 2021. Variable fluid flow regimes alter human brain microvascular endothelial cell-cell junctions and cytoskeletal structure. Cytoskeleton (hoboken) 78, 323–334.
Resnick, N., Cimbrone, M.A., 1995. Hemodynamic forces are complex regulators of endothelial gene expression. FASEB J. 9 (10).
Soon, C.F., Tee, K.S., Youseffi, M., Denyer, M.C.T., 2015. Tracking traction force changes of single cells on the liquid crystal surface. Biosensors 5 (1).
Souilhol, C., Harmsen, M.C., Evans, P.C., Krenning, G., 2018. Endothelial-mesenchymal transition in atherosclerosis. In Cardiovascular Research. 114 (4).
Steward, R.L., Cheng, C.M., Wang, D.L., LeDuc, P.R., 2010. Probing cell structure responses through a shear and stretching mechanical stimulation technique. Cell Biochem. Biophys. 56 (2).
Steward, R., Tambe, D., Corey Hardin, C., Krishnan, R., Fredberg, J.J., 2015. Fluid shear, intercellular stress, and endothelial cell alignment. Am. J. Physiol. Cell Physiol. 308 (8).
Tambe, D.T., Croutelle, U., Trepat, X., Park, C.Y., Kim, J.H., Millet, E., Butler, J.P., Fredberg, J.J., 2013. Monolayer stress microscopy: limitations, artifacts, and accuracy of recovered intercellular stresses. PLoS One 8 (2).
Tang, X., Tofangchi, A., Anand, S.V., Saif, T.A., 2014. A Novel cell traction force microscopy to study multi-cellular system. PLoS Comput. Biol. 10 (6).
Ting, L.H., Jahn, J.R., Sniadecki, N.J., 2012. Flow mechanotransduction regulates traction forces, intercellular forces, and adherens junctions. Biophys. J . 102 (3).
Trepat, X., Wasserman, M.R., Angelini, T.E., Millet, E., Weitz, D.A., Butler, J.P., Fredberg, J.J., 2009. Physical forces during collective cell migration. Nat. Phys. 5 (6).
Wagenseil, J.E., Mecham, R.P., 2012. Elastin in large artery stiffness and hypertension. J. Cardiovasc. Transl. Res. 5 (3).
Wang, J.H.C., Lin, J.S., 2007. Cell traction force and measurement methods. Biomech. Model. Mechanobiol. 6 (6).
Widlansky, M.E., Gokce, N., Keaney, J.F., Vita, J.A., 2003. The clinical implications of endothelial dysfunction. J. Am. Coll. Cardiol. 42 (7).
Zeng, L., Zhang, Y., Chien, S., Liu, X., Shyy, J.Y.J., 2003. The role of p53 deacetylation in p21Waf1 regulation by laminar flow. J. Biol. Chem. 278 (27).
Zhang, W., Smith, C., Shapiro, A., Monette, R., Hutchison, J., Stanimirovic, D., 1999. Increased expression of bioactive chemokines in human cerebromicrovascular endothelial cells and astrocytes subjected to simulated ischemia in vitro. J Neuroimmunol 101, 148–160.